



Obtaining the Manning roughness with terrestrial-remote sensing technique and flood modeling using FLO-2D: A case study Samsun from Turkey

Vahdettin Demir¹ and Asli Ülke Keskin²

¹Department of Civil Engineering, Faculty of Engineering,
KTO Karatay University, Konya, Turkey

²Department of Civil Engineering, Faculty of Engineering,
Ondokuz Mayıs University, Samsun, Turkey

Received 28 May 2020, in final form 9 September 2020

Determining the Manning roughness coefficients is one of the most important steps in flood modeling. The roughness coefficients cause differences in flood areas, water levels, and velocities in the process of modeling. This study aims to determine both the Manning roughness coefficient in the river sections and outside of the river regions by using the Cowan method and remote sensing technique in the flood modeling. In the flood modeling, FLO-2D Pro program which can simulate flood propagation in two dimensions was utilized. Mert River in Samsun province located in the northern part of Turkey was chosen as the study area. Samples taken from the river were subjected to sieve analysis, the types of constituent material were determined according to the median diameters and the roughness coefficients were obtained using the Cowan method. For regions outside of the river were applied the maximum likelihood method being one of the controlled classification methods. Manning roughness values were assigned the classified image sections. Remote sensing techniques were meticulously employed to achieve time management in areas outside the river and a new approach was proposed in the Manning assessment of flood areas to ensure uniformity in the study area. In the classification made using the maximum likelihood method, the overall classification accuracy was 92.9% and the kappa ratio " κ " was 90.64%. The results were calibrated with the last hazardous flood images in 2012 and HEC-RAS 2D program, another flood modeling program.

Keywords: Manning, Cowan method, classification, flood propagation map, FLO-2D; HEC-RAS

1. Introduction

The roughness coefficients measure the resistance to smooth flow in a fluid channel. Hydraulic calculations employed in the design of floodplains of bridges and highways are essential for floodplain management as well as flood insurance

study (Arcement et al., 1984). One of the most significant methods utilized in hydraulic calculations is the Manning method. Irish engineer Robert Manning developed this method (Eq. (1)) in 1889 and it has come to prominence in today's applications.

$$Q = \frac{1}{n} R^{\frac{2}{3}} J^{\frac{1}{2}} A, \quad (1)$$

where:

Q = flow rate, (m³/s),

A = flow area, (m²),

R = hydraulic radius, (m),

n = Manning roughness coefficient (unitless), and

J = slope of the channel at the point of measurement.

Each component of the equation is explained as follows:

Hydraulic radius is the variable related to the channel geometry. The hydraulic radius is computed as the area of flow divided by the flow wetted perimeter. The wetted perimeter is the length of the wetted section around the fluid conduit. Flow area, hydraulic radius, and slope parameters in the Manning equation can be measured physically. When calculating flow rate and velocity, the related parameters are calculated by replacing them in the equation. However, the roughness coefficient (n) is not physically measurable especially in natural river beds, but it is determined empirically according to different criteria. The roughness coefficient (n) is the most important parameter affecting the flow properties in stream beds. Any alteration in this parameter directly affects the result of the hydraulic calculations (DSI, 2016).

The factors influencing the computation of roughness coefficient in the Manning formula were proposed by Chow in 1959 (Chow, 1959), Henderson in 1966 (Henderson, 1966), and Streeter in 1971 (Streeter, 1971). The roughness coefficients and characteristics of natural flow channels for a typical river and stream were explained through photographs by Barnes (Barnes, 1967). Manning tables (Manning, 1891), physical/empirical equations (Limerinos, 1970), calculations of flow velocity measurement (Leopold, 1953), and Cowan method are utilized to determine the roughness coefficient (Cowan, 1956; Arcement and Schneider, 1989). Because Manning tables adopt a practical approach, they are often used to model hydraulic structures in the floodplain (Ülke et al., 2017; Ahn et al., 2019). When utilizing Manning roughness coefficient tables, it was discovered that there are significant differences between the predicted flow velocities and the actual flow velocities in the river (DSI, 2016). This situation can be proved by selecting low roughness values. When Manning roughness coefficient table is used to obtain roughness coefficient, with low roughness values are obtained impossible high velocities (Cowan, 1956). Because many different parameters are affecting the roughness of river beds (bridge pier, tree, meandering, etc.), the image compression method is not applicable (Barnes, 1967). Though flow veloc-

ity measurement is the best method for evaluating the roughness coefficient, it is a time-consuming method because the flow is not always visible and measurement difficulties are prevalent in the cross-section (Ladson et al., 2002). However, this method can be utilized to calibrate the roughness values obtained from other methods. Since the coefficients obtained from physical experiments are often obtained in uniform conditions, they cannot give precise results in non-uniform river beds.

While determining the velocity and flow rate of artificial and natural channels, the hydraulic radius (R) and the slope of the channel cross-section are utilized. Later, Manning's coefficient " n " is selected, and the modeling is carried out. In artificial channels, this selection is relatively easy. The values depending on the channel coating can be selected. While evaluating the velocity and flow rate of natural streams, a coefficient " n " is also chosen. The choice of the roughness coefficient depends on the knowledge, experience, and predictive ability of the researcher making the selection. The coefficient " n " varies according to the roughness characteristics of the investigated surface, vegetation, shape, size, and curvature of the section along the channel. It also varies according to the number, shape, and size of the structures built on the river (bridge pillars, regulator, etc.), as well as water level in the cross-section, flow rate and seasonal (temporal) variations of vegetation (Bulu and Yilmaz, 2002).

In the Cowan method, the Manning coefficient is calculated by considering many factors that result in the roughness as described above (Cowan, 1956). Unlike other methods, the Cowan method is applicable in the river region as it takes into consideration the physical, geometrical, and temporal (seasonal changes in the river slope and vegetation level) changes of the river. In areas outside of the river bed such as in floodplains, the study area image obtained by remote sensing techniques was classified using the controlled classification method to ensure uniformity in the study area. Although many studies have been carried out to determine the roughness coefficients for open channel flow (Azmon, 1992; Mohamoud, 1992; Kaiser et al., 2015), studies for flood plains in dense vegetative parts or urban boundaries are limited. The aim of this study is to propose a new procedure involving remote sensing techniques as well as experimental studies to determine the roughness coefficients for river-stream beds and floodplains outside of the river areas. In other words, the objective includes producing a Manning map of the flood areas. The map is also utilized in 2-Dimensional (2D) flood modeling applied for different return periods (Q50, Q100, Q500, and Q1000).

In contrast to general literature including only flood modeling (Tallat et al., 2011; Chinnarasri and Phothiwijit, 2016; Dimitriadis et al., 2016; Khattak et al., 2016; Patel et al., 2017; Afshari et al., 2018) and only Manning value from satellite image (Straatsma and Baptist, 2008; Forzieri et al., 2011; Bates, 2012; Sadeh et al., 2018) or only Manning value from sampling of terrain (Cowan, 1956; Jarsjö et al., 2015), Manning roughness coefficients was obtained by being used remote sensing and modified Cowan method to enhance the modelling accuracy and

these data were also analyzed using photos showing flood level and computational model FLO 2D. The calibration of this model was made with Hydrologic Engineering Center-River Analysis System (HEC-RAS), which has 2D flow simulation functionality. HEC-RAS is the principal model used in the US Federal Emergency Management Agency (FEMA)'s National Flood Insurance Program (FEMA, 2014; Brunner, 2016; U.S. Army Corps of Engineering, 2018) and National Oceanic and Atmospheric Administration (NOAA)'s Advanced Hydrologic Prediction Service especially (NOAA, 2011).

2. Methods

2.1. Determination of the roughness coefficient

In this study, the roughness coefficient was determined by dividing the study area into two sections. The first is the region where the river bed is located, and the second is the urban-rural region outside the river bed. The Manning roughness coefficient was determined using remote sensing techniques in the areas outside of the river, and the Cowan method inside the river.

2.1.1. Cowan method

The method was developed in 1956 by Cowan (Cowan, 1956). It was modified in 1989 by the US Geological Survey (Arcement et al., 1984). Moreover, (n_1) parameters were developed by Turkey's General Directorate of state Hydraulic Works (DSI) (DSI, 2016). The Cowan method equation is as follows:

$$n = (n_b + n_1 + n_2 + n_3 + n_4)m. \quad (2)$$

In this equation, n_b is the coefficient chosen according to the ground characteristics of the channel, n_1 is the coefficient chosen according to the type of side slope, n_2 is the coefficient determined according to shape and size of channel, n_3 is the coefficient determined for the effect of obstructions in the channel, n_4 is the coefficient selected for flow conditions and vegetation, and m is the coefficient expressing the degree of curvature of the channel (Arcement and Schneider, 1989). The coefficients "n" in Eq. (2) are given in Tab. 1 (Barnes, 1967; DSI, 2016).

The n_b value (median diameter) in Tab. 1 is obtained by a sieve analysis of samples taken from the river area. The n_1 and n_4 value can be determined with the help of field survey and images taken from river sections. River right and left slope conditions (concrete wall, stone wall and vegetation in the channel low or middle etc.) are examined in the images and the roughness coefficients determined using the proportion. The n_2 and m value can be determined with the help of the plan image in Fig. 2 and n_3 value with the help of both plan and section images. The slope % values in Tab. 1 are calculated with $(\text{obstacle} / \text{section area}) \times 100$. The channel fold values are obtained by proportioning $(\text{the length of the river}) / (\text{river air distance})$. Then, the m value in the corresponding range is selected.

Table 1. Modified Cowan method “n” values.

Type of material on the river bed	Concrete	–		0.012–0.018	
	Rock	–		–	
	Soil	–		0.025–0.032	
	Grit	1–2		0.026–0.035	
	Fine gravel	Median diameter	–	n_b	–
	Gravel		2–64		0.028–0.035
	Coarse gravel		–		–
	Coarse stone		64–256		0.030–0.050
	Big rock		>256		0.040–0.070
Channel side slope	Smooth	–		0.000	
	Insignificant	Concrete wall		0.003	
		Stone wall		0.005	
		Stacking stone support	n_1	0.008	
	Middle	Soil slope		0.010	
	Severe	Stacked stone support		0.015	
Tree slope			0.020		
Channel section change	Gradual			0.000	
	Occasionally changing		n_2	0.005	
	Frequently changing			0.01–0.015	
Obstacles in the channel	Neglected	< 5%		0.000	
	Insignificant	5–15%	n_3	0.01–0.015	
	Noteworthy	15–50%		0.02–0.03	
	Severe	> 50%		0.04–0.06	
Vegetation in the channel	Low			0.005–0.010	
	Middle		n_4	0.010–0.025	
	High			0.025–0.050	
	Very high			0.050–0.100	
Channel fold	Insignificant	1–1.2		1.000	
	Noteworthy	1.2–1.5	m	1.150	
	Severe	> 1.5		1.300	

2.1.2. Remote sensing techniques and image classification

The maximum likelihood method is a controlled classification method that is widely used in the classification of satellite images. This method is a statistical-based classification algorithm and performs the classification considering the variance, covariance and mean of image reflection values. In the method, the data forming the class control sets and the pixels to be classified are assigned to the classes with the highest probability of membership (Günlü, 2012). If the probability values for the classes calculated for the pixels are below the threshold value previously determined, the relevant pixels are classified as indefinite (Bulut and Günlü, 2016). The maximum likelihood method equations are as follows (Topaloglu et al., 2016):

$$P(x) = \ln(a_c) - 0.5 \ln(|S_x|) - 0.5(x - M_x)^T (S_x^{-1})(x - M_x), \quad (3)$$

$$M_x = \frac{1}{K} \sum_{k=1}^K x_k, \quad (4)$$

$$S_x = \frac{1}{K-1} \sum_{k=1}^K [(x - M_x)^T (x - M_x)]. \quad (5)$$

In Eqs. (3), (4) and (5) P represents the probability value, C represents an exemplary class, x is the measurement vector of the candidate pixel, M is the average of the class, a_c is the percentage of the candidate pixel belonging to the class, K is the total number of pixels in a class and S_x is the variance-covariance matrix (Myung, 2003).

2.2. Hydraulic modeling – FLO-2D

In this study, flood maps were obtained by using FLO-2D Pro software (FLO-2D, 2018), which can perform flood simulation in two dimensions. The propagation of the flood wave over the flow area varies depending on the topography and flow barrier elements. Flood modeling in two dimensions is carried out by conservation of volume for sediment flow or water flow and numerical integration of motion equations. In FLO-2D, the equations of motion include the continuity equation and the momentum equation (Kim et al., 2012; Haile et al., 2018):

$$\frac{\partial h}{\partial t} + \frac{\partial hV}{\partial x} = 1, \quad (6)$$

$$S_f = S_0 - \frac{\partial h}{\partial x} - \frac{V}{g} \frac{\partial V}{\partial x} - \frac{1}{g} \frac{\partial V}{\partial t}. \quad (7)$$

In Eqs. (6) and (7) h is the depth of flow, V is the average velocity dependent on depth, i is the precipitation intensity, S_f is the energy slope component (based on Manning equation), and S_0 is the river bed slope. These equations are for one-dimensional average channel current. For the flood area, while the FLO-2D is a multidirectional flow model, the motion equations in FLO-2D are applied by calculating the average flow rate along a grid element boundary in one direction over time. One grid element has eight flow directions, four of which are compass directions (north, east, south, and west), and the other four are diagonal directions (northeast, southeast, southwest, and northwest). Each speed calculation is one-dimensional and independent of the other seven directions. Since each grid element for the flow is associated with another grid element, speed vectors do not need to be separated into components. The addition of pressure components to obtain the wave equation makes it possible to perform surface flow simulation in complex topography. The pressure component in wave equation is

necessary to predict how the flood wave will be damped and the change in storage in the flood bed. In the FLO-2D model, only the full dynamic wave equation is applied (FLO-2D, 2018).

3. Case study and data

Mert River is located in the center of Samsun. Samsun province generally shows a topographic structure consisting of a low plateau and mountains. Samsun province's coordinates are 41.279° N and 36.336° E. This area faces devastating floods which have a destructive effect on humans, buildings, and substructure systems. The Mert River, which is approximately 8 kilometers long, flows into the Black Sea and has five highway bridges and one pedestrian bridge. Mert River was selected for this study because the area faced a great loss of life and property in the recent floods (e.g., July 3, 2012) (Ülke et al., 2017; Beden et al., 2018). The study area is shown in Fig. 1.

Black Sea climate prevails in the region. Winters are mild and rainy, summers are quite hot and dry. According to the observations of Samsun Regional

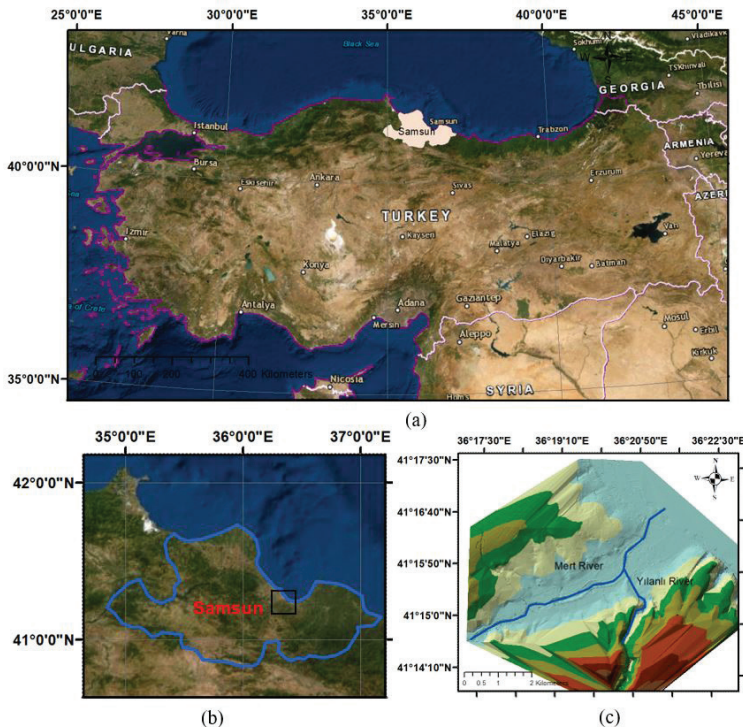


Figure 1. The study area (Location Turkey (a), Samsun Province (b), study area (c)).

Table 2. Location-period informations of precipitation and flow stations.

Station type	Station name	Latitude (°, N)	Longitude (°, E)	Observation period
Meteorological observation stations	Samsun	41.34	36.25	1960–2018
	Mazlumoğlu	40.92	36.02	1959–2012
	Cakıralan	41.17	35.76	1969–1988
Current observation stations	Mert	41.24	36.28	2007–2018
	Engiz	41.48	36.07	1965–2015
	Kürtün	41.23	36.19	1965–2015
	Abdal	41.22	36.57	1968–1991
	Dereçam	41.08	35.96	1973–2015
	Terme	41.08	36.83	1969–2015

Meteorological Station in the period 1929–2018 the average annual temperature is 14.5 °C, the highest temperature is 39 °C with August, the lowest temperature is –9.8 °C with February. The average annual rainfall is 136.4 mm and the total annual rainfall is 717.1 mm. The coastal parts of Samsun province have a typical Black Sea climate. However, the effects of continental climate prevail in the interior. In Samsun, precipitation is less than the Eastern Black Sea and the temperature is high. The coasts are mild in winters, foggy and cool in spring, and dry in summer. Precipitation is usually in the form of rain (Demir and Ülke Keskin, 2019).

In this study, the surface area of the study area was obtained with the help of topographic map. The Manning map base was gotten with the multispectral satellite image acquired by SENTINEL-2. The return flood flow was obtained by using precipitation data and flow data recorded at the observation station in the region. Information about the data is given in Tab. 2.

4. Application and results

4.1. Determination of the roughness coefficient

The first stage in determining the roughness coefficients was to divide the study area into two sub-sections. These are the first sub-section consisting of Mert River and Yılanlı River, and the other sub-section consisting of the urban regions outside the river. Features of the study area were identified such as Manning roughness coefficient of the river bed, Manning roughness, vegetation, channel side-slope, channel curvature, deposition and wear, channel slope. Some factors such as size and shape, level and flow, seasonal variations were also identified. Because of taking these factors into consideration, the Mert River was divided into ten different sections and the Yılanlı River was divided into three different sections (Fig. 2). The roughness coefficients were obtained using the

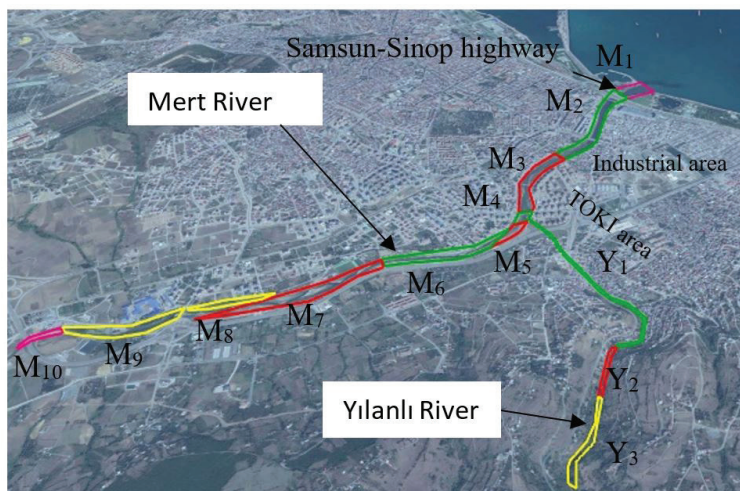


Figure 2. Subdivision of the study area.

Cowan method Eq. (2) in the river section, while remote sensing-image classification techniques Eq. (3) were employed to determine the coefficients in regions outside the river. The aim of this section was to reduce any uncertainty that may occur in the roughness data of the vegetative section of the study area. This increases the reliability in estimating water levels in channels where aquatic vegetation is present. The roughness plays an important role in estimating water level as it reduces the river discharge capacity (Stanciu et al., 2000). This reduction is due to the energy involved in generating boundary turbulence. Also, the roughness is an important factor determinant of water level due to physical conditions obstructing to flow by vegetation.

The steps employed to determine the roughness coefficient of the study area are as follows (Demir and Ülke Keskin, 2019):

Step 1. To begin, the study area where the samples will be collected was examined. In other words, the regions where the roughness values could undergo variation were first inspected. After the examination process, the study area was subdivided into the Mert River and Yılanlı River which is its adjoining tributary. In the construction of these sections, the type of river basement material, the level of vegetation in the river, river fold, degree of slope, and cross-sectional changes were taken into consideration (Fig. 2).

Step 2. It was ensured that the samples required for sieve analysis were taken from the inspected sections in step 1 (Fig. 3a), the samples were dried in the laboratory environment (Fig. 3b) and subjected to sieve analysis (Figs. 3c–3d). In employing the Cowan method, n_b value was determined according to the median diameter obtained from the analysis (Fig. 4).



Figure 3. Sample sampling area (a), drying of samples in the oven (b), sieve shaking table (c), weighing the screened samples (d).

Table 3. “n” values according to Cowan method for $M_1 - M_{10}$ cross sections.

Sample ID	m	n_b	n_1	n_2	n_3	n_4	n
M_1	1	0.015	0.005	–	–	0.005	0.025
M_2	1	0.015	0.005	–	–	0.005	0.025
M_3	1.15	0.033	0.005	0.005	–	0.01	0.061
M_4	1.15	0.015	0.005	0.005	0.01	0.01	0.052
M_5	1.15	0.033	0.005	0.005	0.01	0.01	0.072
M_6	1	0.015	0.005	–	0.01	0.005	0.035
M_7	1	0.033	0.01	–	0.01	0.01	0.063
M_8	1	0.033	0.01	–	0.01	0.01	0.063
M_9	1	0.033	0.01	–	0.01	0.01	0.063
M_{10}	1.15	0.033	0.01	0.005	0.02	0.01	0.090

Step 3. The other parameters used to determine the Manning friction coefficient (Tabs. 3 and 4) and friction values were evaluated using Cowan formula Eq. (2). The images of each region in Fig. 2 and the Manning values determined for each section are shown in Figs. 5 and 6. The results of all sections are enumerated in Tab. 5.

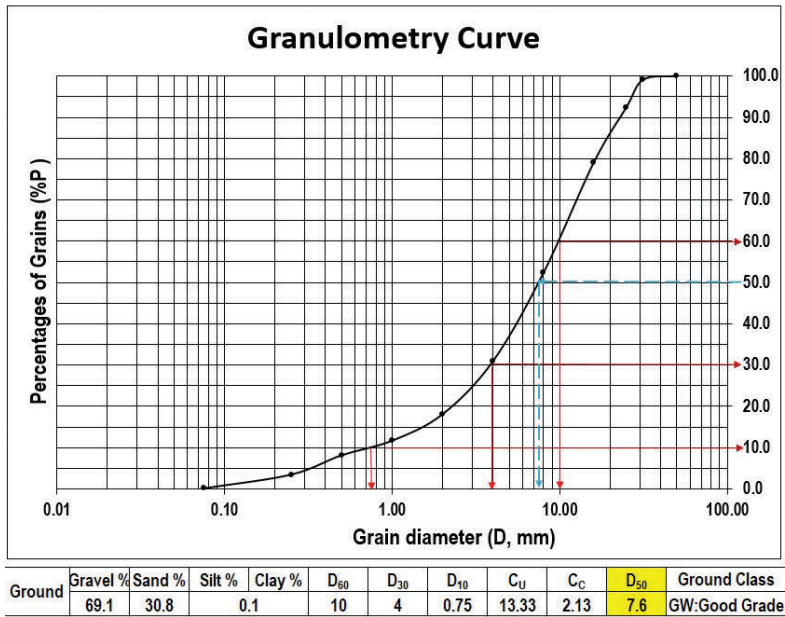


Figure 4. Plotting the granulometry curve and finding the median diameter (for sample M₁).

Table 4. “n” values according to Cowan method for Y₁–Y₃ cross section.

Sample ID	m	n _b	n ₁	n ₂	n ₃	n ₄	n
Y ₁	1	0.015	0.005	–	–	–	0.020
Y ₂	1.15	0.033	0.005	0.005	0.01	0.001	0.072
Y ₃	1.15	0.040	0.01	0.005	0.01	0.01	0.086

Table 5. “n” values according to Cowan method for all cross section.

River	Sample ID	n value
Mert River	M ₁	0.025
	M ₂	0.025
	M ₃	0.061
	M ₄	0.052
	M ₅	0.072
	M ₆	0.035
	M ₇	0.063
	M ₈	0.063
	M ₉	0.063
	M ₁₀	0.090
Yılanlı River	Y ₁	0.020
	Y ₂	0.072
	Y ₃	0.086

M₁



M₂



M₃



M₄



M₅



M₆



M₇



M₈



M₉



M₁₀



Figure 5. M1 – M10 cross sections.



Figure 6. $Y_1 - Y_3$ cross sections.

Step 4. In regions other than the river bed, the roughness values n were determined using satellite image. For this purpose, a SENTINEL-2 image which was acquired on 10.03.2019 at a pixel resolution of 10 meters (Fig. 7) was used for free. SENTINEL-2 measures brightness from 13 visible and near-infrared reflections to short-wave infrared (SWIR) reflections (Anonymous, 2019). Sample

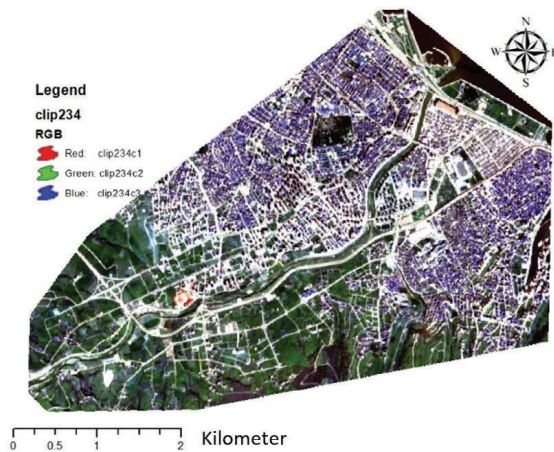


Figure 7. Image of study area SENTINEL-2

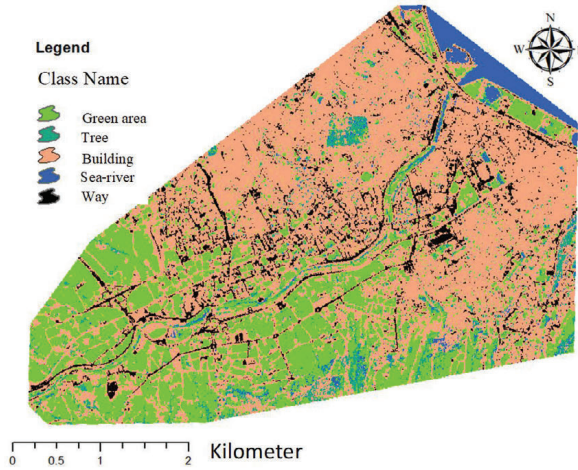


Figure 8. Classified image.

surfaces were taken from the captured image and all images were classified using the maximum likelihood method (Fig. 8). Manning values n for each classified region were determined according to the surface type becoming available in literature (Chaudhry, 2008). The suggested n values include 0.030 in clean and flatlands of natural beds, 0.030–0.035 in plant density, 0.022 in concrete walls, 0.013 in asphalt pavement, 0.016 in rough asphalt, and 0.040 in areas consisting of gravel and coarse rocks (Chow, 1959). In this study, Manning roughness coefficients vary between 0.025 and 0.086.

The classification accuracy of the captured images was determined using kappa value. Accuracy analysis of the image classification was based on the principle of statistical comparison of the image pixel values for each study area rather than those of training sites. These pixel values for the study area are obtained from a source that provides precise information about map or terrain. The kappa value (κ) is a coefficient obtained using a probability matrix and is applied as a statistical measure that predominantly calculates the classification accuracy. Kappa value is calculated using the following equation:

$$\kappa = \frac{N \sum_{i=1}^r x_{ii} - \sum_{i=1}^r x_{i+} x_{+i}}{N^2 - \sum_{i=1}^r x_{i+} x_{+i}} \tag{8}$$

In Eq. (8), r represents the number of classes. The diagonal elements of the error matrix x_{ii} , the sum of the rows x_{i+} , the sum of the column x_{+i} , and the total number of pixels in the error matrix N represents the matrix.

If the kappa value was 75% or more, the classification accuracy was very good, if it was between 40% and 75%, the classification accuracy was medium-

Table 6. Error matrix for test areas.

Class name	Class no.	1	2	3	4	5	Total
Green area	1	32	0	0	0	0	32
Tree	2	1	18	0	1	0	20
Building	3	2	0	28	0	1	31
Sea-river	4	0	0	0	6	0	6
Way	5	0	0	3	0	20	23
Total		35	18	31	7	21	112

good and if it was below 40%, the classification accuracy was regarded as weak (Ayhan et al., 2007).

Errors in classification are caused by incorrect classification of image pixels. If sufficient number of pixels are not classified on the image, the rate of representing the reality of the data sets decreases. In this study, the Kappa value was obtained for the classified image in ArcGIS program. Error matrix of classification reference data is given in Tab. 6.

The i^{th} element (i^{th} diagonal element) of row “ i ” of the matrix contains the number of pixels correctly labeled by the classifier and included in class “ i ” by the operator. Elements in other columns of the same row show the number and distribution of pixels that have been incorrectly classified. The accuracy degree

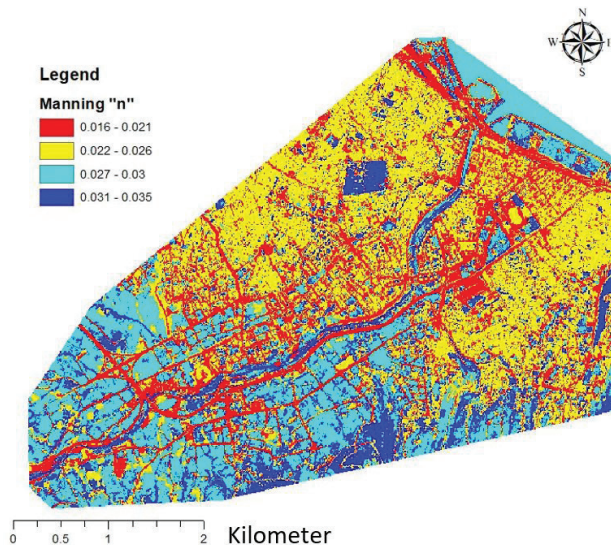


Figure 9. Distribution of roughness coefficients.

of class “*i*” is obtained by dividing the diagonal element by the reference data sum of the same row. The overall classification accuracy (as a percentage) is the average of each class’s accuracy (Mather, 1999). The overall classification accuracy for Tab. 6 is $(110 / 112) \times 100 = 0.929$.

The kappa value summarizing the information provided by the error matrix is used as a statistical measure that mainly calculates the accuracy of the classification. The kappa value (Eq. 8) for the values in Tab. 6 was calculated as follows:

$$\kappa = \frac{112 \times 104 - 2,966}{12,544 - 2,966} = 0.9064 .$$

In Fig. 9, the Manning value was low in urban areas (red-yellow areas), while it was high both in river bed and rural-wooded areas (light blue-dark blue). In the classification made using the maximum likelihood method, the overall classification accuracy was 92.9% and the kappa ratio was found to be 90.64%.

4.2. Flood modeling and flood mapping

After the Manning map was obtained, the flood modeling phase commenced. FLO-2D was utilized for hydraulic analysis and ArcGIS 10.2 was employed for mapping. Firstly, flood return periods were calculated with DSI Synthetic method, Mockus method, Snyder method, and Local – Regional Flood Frequency Analysis (FFA) for 5 similar stations (Engiz – D15A026, Kürtün – D14A014, Abdal – D14A042, Dereçam – D14A081, Terme – E22A045). Secondly, Digital Elevation Map (DEM) was created using topographic maps. The resolution of DEM is 25 meters and it was created in ArcGIS. Finally, hydraulic modeling was performed using DEM, flood return and Manning map. The purpose of calculating the return periods was to determine using various methods, the different flood recurrence flow rates that were likely to occur in the study area. The optimum height of the flood cross-section was found using determined flow rates. To dimension hydraulic structures such as bridges, culverts, dams, regulators, and flood traps, and to take precautions against possible floods (structural and non-structural), it was necessary to predict the flow rates using various return periods. This is only possible with the use of statistical or deterministic methods. In this way, it will be possible to determine the risk associated with the use of floodplain and provide necessary solutions through the design of hydraulic structures. The flood return periods were calculated using deterministic methods such as DSI Synthetic method, Mockus method, Snyder method, and Local - Regional Flood Frequency Analysis in case of insufficient precipitation-flow data. Details of the methods were presented by Bayazit et al. (2002). These methods were chosen because Mert River lacked enough flow data for statistical analysis (Tab. 2). Also, the observation station was not available on the Yılanlı River. The Mockus between 0–10 km², DSI Synthetic between 10–1,000 km², and Snyder methods for

Table 7. Return periods summary table.

Return periods (m ³ /s)	Local flood frequency analysis					Regional FFA	Mocus	DSI Synthetic	Snyder
	D15A026	D14A014	D14A042	D14A081	E22A045				
Q2	201.8	92.9	143.2	63.7	531.4	155.0	337.6	295	312.5
Q5	392.5	204	282.9	146.4	892.9	313.0	502.4	433	464.5
Q10	561.6	307.4	402.3	224.2	1,181.9	454.1	639.8	548	591.3
Q25	829	475.5	584	351.4	1,604.4	677.2	855.8	729	790.7
Q50	1,070.2	629.9	741.7	467.9	1,960.8	877.5	1,053.7	895	973.3
Q100	1,351.1	810.3	918	603.5	2,355.6	1,108.1	1,294.2	1,098	1,195.3
Q500	2,079.1	1287	1,356.9	960.6	3,308.2	1,703.5	1,962.4	1,659	1,811.9
Q1000	2,132.4	1,308.1	1,428.3	979.1	3,517.1	1,755.3	1,942.2	2,216	1,793.2

drainage areas larger than 1,000 km² were recommended. Since the Mert River's basin area is 810 km², it was necessary to adopt the DSI Synthetic method. Also, it was concluded to use the Mocus method since the basin area of Yılanlı River is 31 km². These methods have been accepted by many researchers when calculating flood flow rates (Hadadin et al., 2013; Kumanlıoğlu and Ersoy, 2018). Besides, the results obtained through these methods are very close to the regional flood analysis rates calculated using other station data (Tab. 7). This was another important factor considered in the selection of these methods.

In this research, it was also important to determine the river base flow. The base flow refers to the average consumption of a stream during the flood time. Depending on the condition of the drainage area and climatic conditions, the base flow varies between certain limits throughout the year. Generally, it is high during winter and spring seasons and low during summer and autumn seasons in areas where snow melts and precipitation are high. In drainage areas with heavy rainfall and snow melting occurring for a long period, the effect of base flow on flood intensity is significant. With this understanding, the base flow should be added to the flood flow where the superficial flow is calculated using synthetic methods (Ozdemir, 1978). An approach for estimating base flow was also proposed by DSI. This approach involves drawing a current-time curve for the average monthly flow currents of the river and the flow current that occurs at 95% of the time is considered as the base flow. Flow data water yearbook starts in October and terminates in September. The graph of the monthly average flow data was visualized in Fig. 10.

The flow-continuous curve of the monthly average flow was based on the current-confidence relationship. Flow current continuous curves were artificially arranged by ordering the obtained current data from small to large.

The order (m) of artificial sequence data was determined. The ranking commenced with the smallest of the artificial sequential current data to be given a value of 1. The confidence (g) values were calculated as a percentage based on

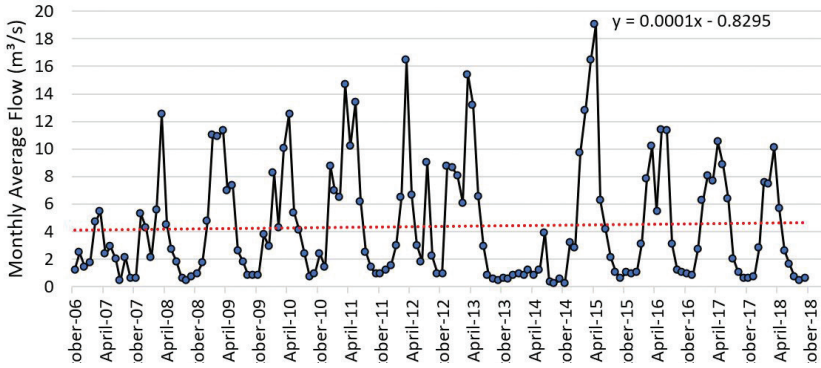


Figure 10. The graph of the monthly average flow for Mert River (station no: E22A062).

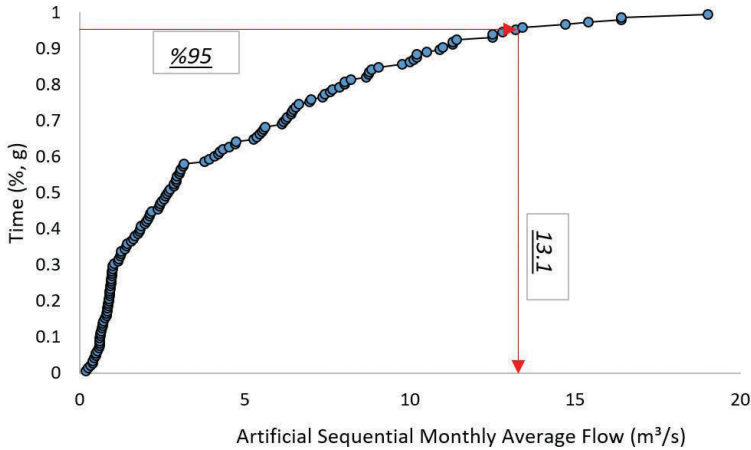


Figure 11. Flow-continuous curve for Mert River (station no: E22A062).

the number of data (n) and the order (m). The confidence value for each rank was obtained using Eq. (9):

$$g = \frac{m}{n + 1} \tag{9}$$

After the confidence values were obtained for each order, current-confidence or current continuous graph was plotted. The flow-continuous curve of the Mert River between the years 2007–2018 is illustrated in Fig. 11.

A base flow value of 13.1 m³/s was obtained and added continuously to the hydrographs which consisted of surface flow calculated using synthetic methods along the hydrograph base (Saka and Yüksek, 2018). The final hydrographs of the obtained repetition flow rates are given in Fig. 12.

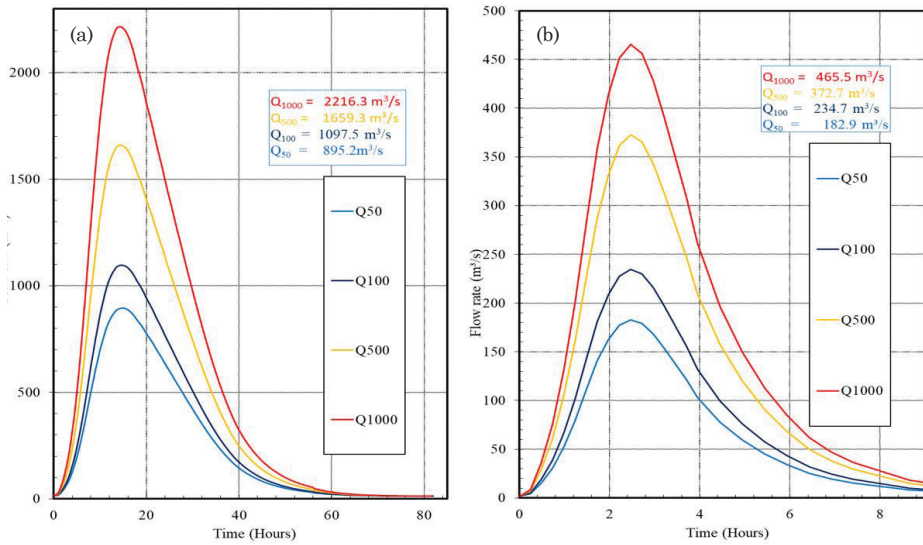


Figure 12. Flood return flows: (a) Mert river, (b) Yılanlı river.

Water levels of flow rates were determined using the FLO-2D package program. For the mapping process, the data was transferred to the *Mapper++* program, a sub-software of the FLO-2D program package. Thus, flood propagation maps (scenarios) of flood flow with return periods including 50 years, 100 years, 500 years, and 1000 years were obtained (Figs.13 and 14).

In Fig. 14, it is visible that the river overflowed from the bed at the 50- year return period and departed the industrial zone of the right side of the study area toward the downstream region. In Fig. 13, it is obvious that the water flow can-

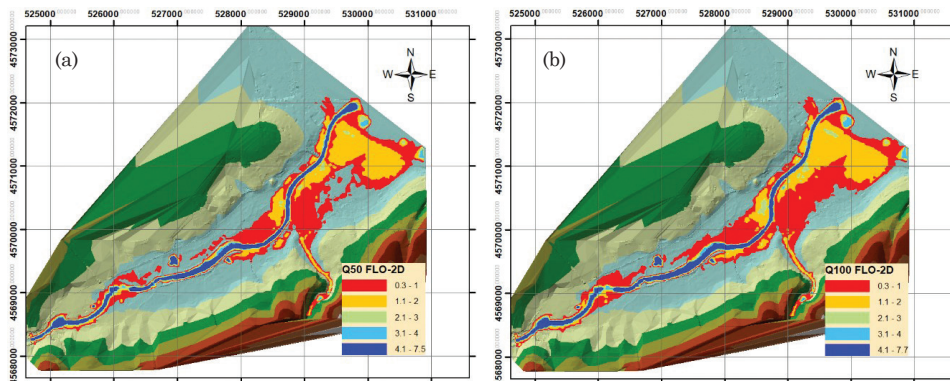


Figure 13. Flood inundation maps of 50 (a) and 100 year (b) return periods.

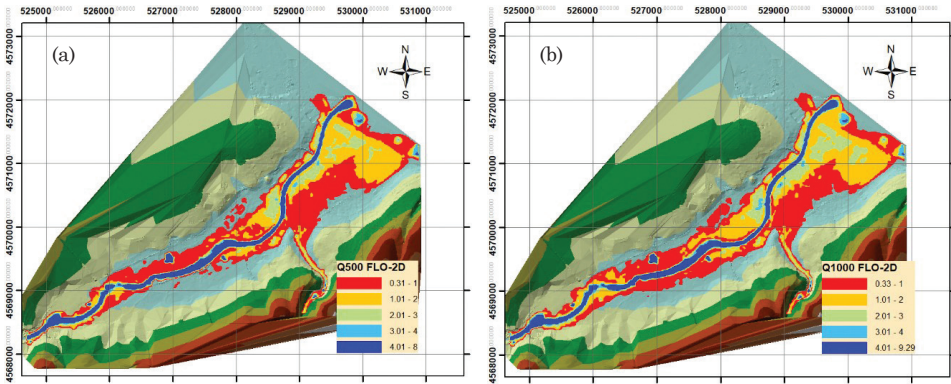


Figure 14. Flood inundation maps of 500 (a) and 1000 year (b) return periods.

not travel through the river folds at Q100 and later Q500 flows and reaches heights up to 2 meters on the right and left sides of the river section. When Figs. 13 and 14 were examined, it was observed that the water levels increased in the industrial and TOKI regions up to 2–3 meters. Besides, water level is maximum 9.29 meters in the middle sections toward the upstream of the Yılanlı River. In all flood scenarios, overflows were prevalent especially in eastern regions of the river. Elevations of right side of the Mert River’s downstream are lower than the other sides. Thus, it is affected by flood with 50 and 100-year return periods. In addition, floods with 50 and 100-year return periods inhibit travel from Samsun-Sinop inter-city highway line to the Black Sea. This eventually results in flooding in the industrial zone. Results, 1D and 2D flood modeling obtained using the

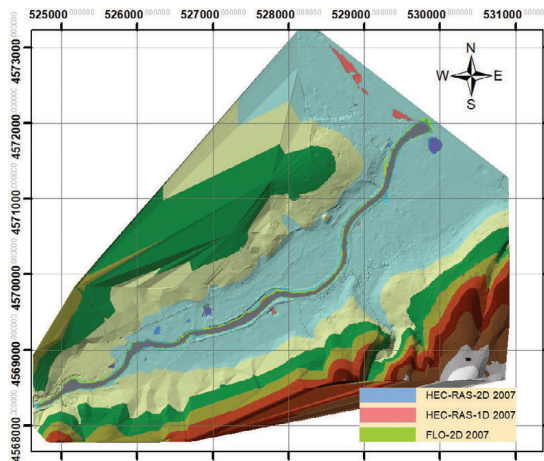


Figure 15. Comparison of the instantaneous maximum flows value in 2007.

MIKE program, (Ülke et al., 2017; Beden and Keskin, 2020) , were similar to the this study. The flood propagation areas generated using the flood repetition flow rates are outlined in Tab. 8.

Table 8. Comparison of flood propagation areas.

Return flow rate (m ³ /s)	Flood propagation area (km ²)		HECRAS 2D
	HECRAS 2D	FLO-2D	FLO-2D
Q50	3.93	4.38	90%
Q100	4.16	4.59	96%
Q500	4.88	5.44	93%
Q1000	5.33	5.93	93%

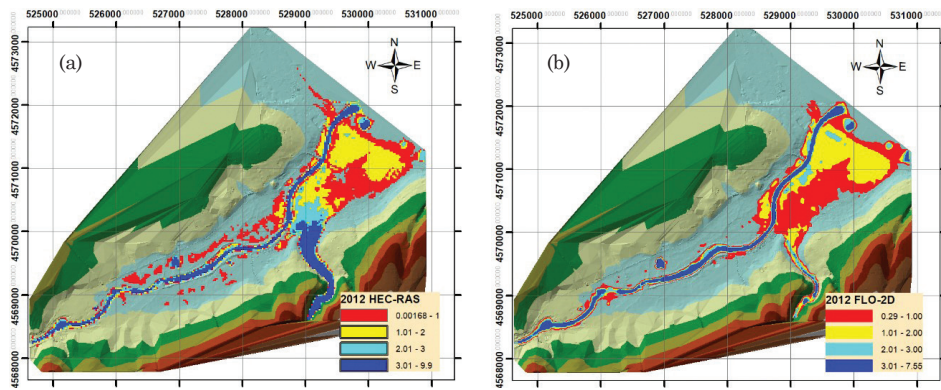


Figure 16. 2012 flood comparison: (a) HEC-RAS, (b) FLO-2D.

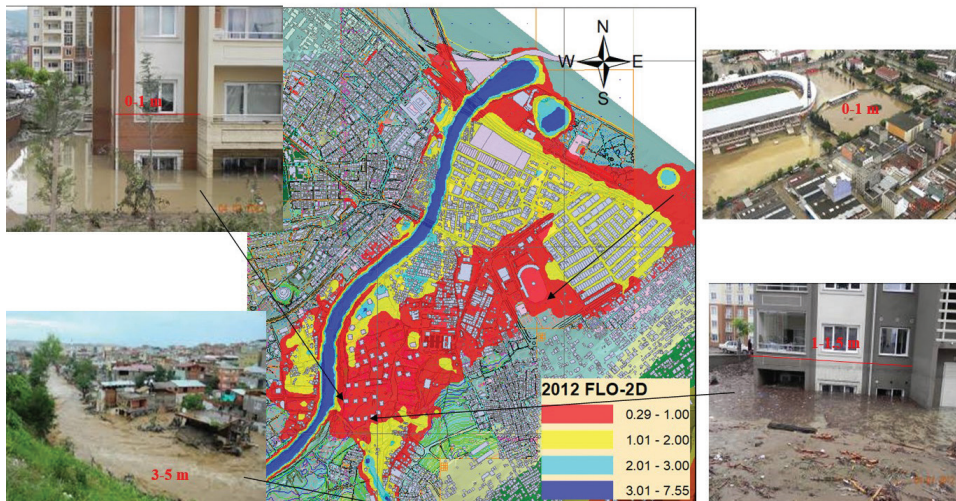


Figure 17. Model calibration with flood image.

All these results were compared with results obtained using HEC-RAS, which was the second package program, and field similarity was determined between 90% and 96% among the two programs. These similarity ratios were calculated with the flood areas used in the modeling of return period flow rates, instantaneous maximum flows between 2007–2018 (for 2007 is given Fig. 15) and flood flow rates in 2012 (570 m³/s for Mert River, 710 m³/s for Yılanlı River, Fig. 16).

The levels determined using past flood trace images were compared with the package program levels (Fig. 17). The simulation results were compared with observed flood extent photos.

5. Discussion and conclusion

In this study, the roughness coefficients representing the resistance against flood flows in open channels and needed in the management of flood areas, in flood insurance studies was determined. Also, flood propagation areas of different return periods were determined using the obtained Manning coefficients.

Manning roughness coefficients were obtained using remote sensing techniques and modified Cowan method. The Cowan method is supported with sieve analysis in vegetation areas such as shrubs and woodlands which are difficult to identify in current maps or not found at all. During the application of method, the report named “Roughness Coefficient Determination Guide for Stream Beds” published by the General Directorate of State Hydraulic Works was used (DSI, 2016). In the process of image classification, the controlled classification method was employed because the number of classes was known and the education areas taken from each class were available. The controlled classification method was also adopted because it provided more accurate results than other methods (Ayhan et al., 2007). Bulut and Günlü (2016) carried out a classification study on land use and they stated that the most successful method among the compared controlled classification methods was the likelihood method. In the classification made using the maximum likelihood method, the overall classification accuracy was 92.9% and the kappa ratio was found to be 90.64%. If the obtained kappa value is greater than 0.75, the classification performance is considered to be very good (Ayhan et al., 2007). Thus, it is think that classification performance is very good in this study.

Flood modeling, which was the second objective of the study, was carried out with the FLO-2D package program which has perform 2D flood modeling for different (Q50, Q100, Q500, and Q1000) flood return periods. The FLO-2D model was employed for the first time in the region in literature. In the analysis, DEM were generated from the terrestrial maps. Statistical methods were employed to acquire these flood return periods. River section information was obtained from the General Directorate of State Hydraulic Works. Manning roughness coefficients were determined through area observations, river sampling,

and satellite image. The FLO-2D package program combined these data generated flood maps. With the Q100 flow rate, approximately 80% of the industrial zone was affected by this flood.

Because the high volume of floods with flow rates close to Q50 and even Q100 flow rates were observed in studies conducted for the Black Sea Region, control measures should be installed in urban areas this flow rates. Figs. 13 and 14 are visualized cross-sections that can lift water up to a height of maximum 9.29 meters in the upstream parts of the study area. Accordingly, adequate cross-section arrangements can be made by increasing the height of the right and left slope of the river at the exit regions of the Mert River to direct the flood into the Black Sea. Flood propagation maps have shown that Samsun-Sinop highway transportation results in the flood in the industrial zone, and the flow channels that constructed on this road were believed to help convey the incoming water to the Black Sea during the incidence of flooding. After applied the Q50 flow, it was observed that the area located in the downstream part of the Mert River was significantly affected by the flood.

Conflict of interest statement – The authors have no conflicts of interest in relation to this study.

References

- Afshari, S., Tavakoly, A. A., Adnan, M., Zheng, X., Follum, M. L., Omranian, E. and Fekete, B. M. (2018): Comparison of new generation low-complexity flood inundation mapping tools with a hydrodynamic model, *J. Hydrol.*, **556**, 539–556, <https://doi.org/10.1016/j.jhydrol.2017.11.036>.
- Ahn, J., Na, Y. and Park, S. W. (2019): Development of two-dimensional inundation modelling process using MIKE21 model, *KSCE J. Civ. Eng.*, **23**, 3968–3977, <https://doi.org/10.1007/s12205-019-1586-9>.
- Anonymous (2019): Multi spectral instrument (MSI) overview, <https://earth.esa.int/web/sentinel/technical-guides/sentinel-2-msi/msi-instrument> (last accessed 26 June 2019).
- Arcement, G. J., Schneider, J. and Schneider, V. R. (1984): *Guide for selecting Manning's roughness coefficients for natural channels and flood plains, Final report*. U.S. Department of Transportation, Virginia, 72 pp.
- Ayhan, E., Atay, G. and Erden, O. (2007): The effect of geometric correction on classification results in high resolution satellite images, in: *Turkey's National Photogrammetry and Remote Sensing Technical Symposium*. İstanbul, Türkiye, 1–5 pp (in Turkish).
- Azmon, B. (1992): Manning coefficient of roughness - A case study along Soreq stream, *J. Hydrol.*, **132**, 361–377, [https://doi.org/10.1016/0022-1694\(92\)90186-Y](https://doi.org/10.1016/0022-1694(92)90186-Y).
- Barnes, H. H. (1967): *Roughness characteristics of natural channels*. Federal Center, Denver, 213 pp.
- Bates, P. D. (2012): Integrating remote sensing data with flood inundation models: How far have we got?, *Hydrol. Process.*, **26**, 2515–2521, <https://doi.org/10.1002/hyp.9374>.
- Bayazit, M. and Oğuz, B. (2018): *Probability and statistics for engineers*. Birsen Publishing, İstanbul, 178 pp.
- Beden, N., Demir, V. and Ülke Keskin, A. (2018): Flood modeling of Samsun / Atakum Region by GIS tools, *J. New Results Sci.*, **7**, 1–8.

- Beden, N. and Ülke Keskin, A. (2020): Flood hazard assessment of a flood-prone intensively urbanized area - A case study from Samsun Province, *Geofizika*, **37**, 1–31, <https://doi.org/10.15233/gfz.2020.37.2>.
- Brunner, G. W. (2016): *HEC-RAS River Analysis System. 2D Modeling User's Manual Version 5.0.*, Davis, 71 pp.
- Bulu, A. and Yılmaz, E. (2002): Determination of roughness coefficient in free surface flows, *Turkey Engineering News*, **420**, 421–423 (in Turkish).
- Bulut, S. and Günlü, A. (2016): Comparison of different supervised classification algorithms for land use classes, *Kastamonu Univ., Journal of Forestry Faculty*, **16**, 528–535, <https://doi.org/10.17475/kastorman.289762>.
- Chaudhry, M. H. (2008): *Open-channel flow*. Springer, Boston, 523 pp.
- Chinnarasri, C. and Phothiwijit, K. (2016): Appropriate engineering measures with participation of community for flood disaster reduction: Case of the Tha Chin Basin, Thailand, *Arab. J. Sci. Eng.*, **41**, 4879–4892, <https://doi.org/10.1007/s13369-016-2166-7>.
- Chow, V. T. (1959): *Open channel hydraulics*. McGraw-Hill, New York, 700 pp.
- Cowan, W. L. (1956): Estimating hydraulic roughness coefficients, *Agr. Eng.*, **37**, 473–475.
- Demir, V. and Ülke, A. (2019): Determination of Manning roughness coefficient by Cowan method and remote sensing, *Gazi J. Eng. Sci.*, **5**, 167–177, <https://doi.org/10.30855/gmbd.2019.02.06>.
- Dimitriadis, P., Tegos, A., Oikonomou, A., Pagana, V., Koukouvinos, A., Mamassis, N., Koutsoyianis, D. and Efstratiadis, A. (2016): Comparative evaluation of 1D and quasi-2D hydraulic models based on benchmark and real-world applications for uncertainty assessment in flood mapping, *J. Hydrol.*, **534**, 478–492, <https://doi.org/10.1016/j.jhydrol.2016.01.020>.
- DSI (2016): *Roughness coefficient determination guide for stream beds*. Ministry of Forestry and Water Management, Ankara, 21 pp.
- FEMA (2014): *Guidance for flood risk analysis and mapping—Flood risk assessments*. Federal Emergency Management Agency (FEMA), Washington, DC, 26 pp.
- FLO-2D (2018): *User's manual (v. 2006.01)*. FLO-2D Software, Inc., Nutrioso, USA, 183 pp.
- Forzieri, G., Degetto, M., Righetti, M., Castelli, F. and Preti, F. (2011): Satellite multispectral data for improved floodplain roughness modelling, *J. Hydrol.*, **407**, 41–57, <https://doi.org/10.1016/j.jhydrol.2011.07.009>.
- Günlü, A. (2012): Estimation of certain stand type parameters (growth stage and crown closure) and land cover using landsat TM satellite image, *Kastamonu Univ., Journal of Forestry Faculty*, **12**, 71–79 (in Turkish).
- Hadadin, N., Tarawneh, Z., Shatanawi, K., Banihani, Q. and Hamdi, M. R. (2013): Hydrological analysis for floodplain hazard of Jeddah's Drainage Basin, *Arab. J. Sci. Eng.*, **38**, 3275–3287, <https://doi.org/10.1007/s13369-013-0812-x>.
- Haile, S., Worku, H. and Paola, F. D. (2018): Flood hazard mapping using FLO-2D and local management strategies of Dire Dawa city, Ethiopia, *J. Hydrol. Reg. Stud.*, **19**, 224–239, <https://doi.org/10.1016/j.ejrh.2018.09.005>.
- Henderson, F. M. (1966): *Open-channel flow*. MacMillan Publishing Co. Inc., New York, 522 pp.
- Jarsjö, J., Romanchenko, A. O., Chalov, S. R. and Pietron, J. (2015): Model analyses of the contribution of in-channel processes to sediment concentration hysteresis loops, *J. Hydrol.*, **527**, 576–589, <https://doi.org/10.1016/j.jhydrol.2015.05.009>.
- Kaiser, A., Neugirg, F., Haas, F., Schmidt, J., Becht, M. and Schindewolf, M. (2015): Determination of hydrological roughness by means of close range remote sensing, *Soil*, **1**, 613–620, <https://doi.org/10.5194/soil-1-613-2015>.
- Khattak, M. S., Anwar, F., Saeed, T. U., Sharif, M., Sheraz, K. and Ahmed, A. (2016): Floodplain mapping using HEC-RAS and ArcGIS : A case study of Kabul River, *Arab. J. Sci. Eng.*, **41**, 1375–1390, <https://doi.org/10.1007/s13369-015-1915-3>.
- Kim, H. J., Lee, J. W., Yoon K. S. and Cho, Y. S. (2012): Numerical analysis of flood risk change due to obstruction, *KSCE J. Civ. Eng.*, **16**, 207–214, <https://doi.org/10.1007/s12205-012-0003-4>.

- Kumanhoğlu, A. A. and Ersoy, S. B. (2018): Determination of flood flows in basins without stream observation: Kizildere Basin Ahmet, *Dokuz Eylül Univ. Eng. J. Sci. Eng.*, **20**, 890–904, <https://doi.org/10.21205/deufmd.2018206070> (in Turkish).
- Ladson, A. R., Anderson, B., Rutherford, I. D. and van de Meene, S. (2002): An Australian handbook of stream roughness coefficients: How hydrographers can help, *Aust. Hydrogr.*, **6**, 4–12.
- Leopold, L. B. (1953): Downstream change of velocity in rivers, *Am. J. Sci.*, **251**, 606–624., <https://doi.org/10.2475/ajs.251.8.606>.
- Limerinos, J. T. (1970): *Determination of the manning coefficient from measured bed roughness in natural channels determination of the manning*. Water Supply Pap 1898-B 47, U.S. Government Printing Office, Washington, 53 pp.
- Manning, R. (1891): On the flow of water in open channels and pipes, *Trans. Inst. Civ. Eng. Irel.*, **20**, 161–207.
- Mather, P. M (1999): *Computer processing of remotely-sensed images*. 2nd edition, John Wiley and Sons, New York, 53 pp.
- Mohamoud, Y. M. (1992): Evaluating Manning's roughness coefficients for tilled soils, *J. Hydrol.*, **135**, 143–156, [https://doi.org/10.1016/0022-1694\(92\)90086-B](https://doi.org/10.1016/0022-1694(92)90086-B).
- Myung, I. J. (2003): Tutorial on maximum likelihood estimation, *J. Math. Psychol.*, **47**, 90–100, [https://doi.org/10.1016/S0022-2496\(02\)00028-7](https://doi.org/10.1016/S0022-2496(02)00028-7).
- NOAA (2011): *NOAA partnered guidelines, for the development of advance hydrologic prediction service flood inundation mapping*. Dewberry, 65 pp.
- Ozdemir, H. (1978): *Applied flood hydrology*. General Directorate of State Hydraulic Works Ankara, Turkey (in Turkish).
- Patel, D. P., Ramirez, J. A., Srivastava, P. K., Bray, M. and Han D. (2017): Assessment of flood inundation mapping of Surat city by coupled 1D/2D hydrodynamic modeling: A case application of the new HEC-RAS 5, *Nat. Hazards*, **89**, 93–130, <https://doi.org/10.1007/s11069-017-2956-6>.
- Sadeh, Y., Cohen, H., Maman, S. and Blumberg, D. G. (2018): Evaluation of Manning's roughness coefficient in arid environments by using SAR backscatter, *Remote Sens.*, **10**, 1–14, <https://doi.org/10.3390/rs10101505>.
- Saka, F. and Yükses, Ö. (2017): Regionalisation of discharges having certain exceedance probabilities and Eastern Black Sea Basin sample, *J. Fac. Eng. Archit. Gaz.*, **32**, 335–342, <https://doi.org/10.17341/gazimmfd.322154>.
- Stanciu, D., Marinescu, M. and Isvoranu, D. (2000): Second law analysis of the turbulent flat plate boundary layer, *Int. J. Thermodyn.*, **1**, 357–366, <https://doi.org/10.5541/ijot.38>.
- Straatsma, M. W. and Baptist, M. J. (2008): Floodplain roughness parameterization using airborne laser scanning and spectral remote sensing, *Remote Sens. Environ.*, **112**, 1062–1080, <https://doi.org/10.1016/j.rse.2007.07.012>.
- Streeter, V. L. (1971): *Fluid mechanics*. McGraw-Hill Book Company, New York, 751 pp.
- Tallat, Q., Siddiqui, M. and Nisar, H. (2011): Flood inundation modeling for a watershed in the Pothwar Region of Pakistan, *Arab. J. Sci. Eng.*, **36**, 1203–1220, <https://doi.org/10.1007/s13369-011-0112-2>.
- Topaloğlu, R. H., Sertel, E. and Musaoğlu, N. (2016): Assessment of classification accuracies of Sentinel-2 and Landsat-8 data for land cover/use mapping, *Int. Arch. Photogramm Remote Sens. Spat. Inf. Sci.*, **41**, 1055–1059, <https://doi.org/10.5194/isprsarchives-XLI-B8-1055-2016>.
- U.S. Army Corps of Engineering (2018): *HEC-RAS 5.0 supplemental to user's manual*. US Army Corps of Engineers Institute for Water Resources Hydrologic Engineering Center, Davis, 74 pp.
- Ülke, A., Beden, N., Demir, V. and Menek, N. (2017): Numerical modeling of Samsun Mert River floods, *EWRA Publ.*, **57**, 27–34.

SAŽETAK

Određivanje Manningove hrapavosti tehnikom daljinskih mjerenja i modeliranjem poplave pomoću modela FLO-2D: primjer Samsun, Turska*Vahdettin Demir i Asli Ülke Keskin*

Određivanje Manningovih koeficijenata hrapavosti jedan je od najvažnijih koraka u modeliranju poplava. Koeficijenti hrapavosti u procesu modeliranja uzrokuju razlike u poplavnim područjima, razinama vode i brzinama. Cilj ove studije je utvrditi koeficijent hrapavosti u riječnim odsječcima te i izvan riječnih područja korištenjem Cowanove metode i tehnike daljinskog istraživanja. U modeliranju poplave korišten je program FLO-2D Pro koji može simulirati širenje poplave u dvije dimenzije. Za područje istraživanja odabrana je rijeka Mert u provinciji Samsun koja se nalazi u sjevernom dijelu Turske. Uzorci uzeti iz rijeke analizirani su pomoću sita, gdje su vrste sastavnog materijala određene prema srednjim promjerima, a koeficijenti hrapavosti dobiveni su Cowanovom metodom. Za područja izvan rijeke primijenjena je metoda najveće vjerojatnosti koja je jedna od kontroliranih metoda klasifikacije. Manningove vrijednosti hrapavosti dodijeljene su klasificiranim odsječcima slike. Tehnike daljinskih mjerenja pomno su korištene kako bi se procijenili koeficijenti hrapavosti u područjima izvan rijeke, a novi je pristup predložen u Manningovoj procjeni poplavnih područja kako bi se osigurala ujednačenost na istraživanom području. U klasifikaciji izvedenoj metodom najveće vjerojatnosti, ukupna točnost klasifikacije bila je 92,9%, a kappa omjer “ κ ” 90,64%. Rezultati su kalibrirani prema posljednjim slikama opasnih poplava 2012. godine i HEC-RAS 2D programom, koji je također program za modeliranje poplave.

Ključne riječi: Manning, Cowanova metoda, klasifikacija, karta propagacije poplave, FLO-2D, HEC-RAS

Corresponding author's address: Vahdettin Demir, Department of Civil Engineering, Faculty of Engineering, KTO Karatay University, 42020 Karatay, Konya, Turkey; tel: +90 332 444 1251 (interior 7696), fax: +90 332 202 0044; e-mail: vahdettin.demir@karatay.edu.tr (ORCID: 0000-0002-6590-5658).



This work is licensed under a Creative Commons Attribution-NonCommercial 4.0 International License.